Retrievals of Horizontal Winds from Single-Doppler Clear-Air Data by Methods of Cross Correlation and Variational Analysis

STÉPHANE LAROCHE AND ISZTAR ZAWADZKI

Department of Atmospheric and Oceanic Sciences, McGill University/Cooperative Center for Research in Mesometeorology (CCRM), Montréal, Québec, Canada

(Manuscript received 5 April 1994, in final form 21 October 1994)

ABSTRACT

Four methods for retrieval of the horizontal wind field are described and compared using single-Doppler observations of a sea-breeze front measured during the Convective and Precipitation/Electrification Experiment. The first method examined is the TREC (tracking radar echoes by correlation) technique similar to the one proposed by Tuttle and Foote. Two other methods, similar to TREC, in which wind vectors are estimated by minimizing the difference between successive patterns of reflectivity, are then examined. These methods conceptually link the TREC method and the velocity volume processing (VVP) approach to the variational wind retrieval method described here. The variational formulation uses the conservation of reflectivity and the radial momentum equation as physical constraints and in this way it incorporates the concepts on which TREC and VVP are based. The performance of the methods is compared using the dual-Doppler wind analysis as ground truth. Results show that the variational method can retrieve the wind field with higher resolution than the TREC method.

1. Introduction

The analysis of the horizontal wind field in the planetary boundary layer (PBL) represents an important step for the prediction of severe convective storms (Tuttle and Foote 1990). The new generation of Doppler radars has the capability to measure the reflectivity and the radial velocity in the clear-air PBL. Since severe thunderstorms are frequently associated with convergence lines that develop 20–30 min prior the first echo related to deep convection, the horizontal wind field should be retrieved from the radar observations as fast as possible (two or three time sequences of observations at most) to obtain useful information for nowcasting.

The full potential of combined single-Doppler radar velocities and reflectivity observations has not yet been realized and represents an interesting challenge. Two basic approaches to the problem have been proposed. In the first, algorithms based on conceptual models of air circulation are used to interpret Doppler velocity "signatures" such as the mesocyclone (Brown and Wood 1991). In the second, physical or geometric constraints are combined with the measurements to retrieve the tangential velocity component. We will be concerned here with the latter approach.

Corresponding author address: Dr. Isztar Zawadzki, Dept. of Atmospheric and Oceanic Sciences, McGill University, 805 Sherbrooke Street West, Montréal, Québec, H3A 2K7, Canada.

The assumption of spatial invariance or linearity of the wind field was used to develop the velocity volume processing (VVP) method (Easterbrook 1975; Walteufel and Corbin 1979; Doviak and Zrnić 1993). Cross correlation of radar patterns at different times has been used to track echo motion (Zawadzki 1973; Rinehart 1979; Tuttle and Foote 1990). The conservation of reflectivity in clear-air echoes is implicitly used when radar echoes are used as tracers of wind motion. Alternatively, velocity perturbations can be cross correlated in time to retrieve the horizontal wind field (Smythe and Zrnić 1983). In this case, the frozen turbulence assumption is used in tracking velocity perturbations.

Recently, variational techniques have been used in conjunction with physical constrains to retrieve two- or three-dimensional air motions from single-Doppler data (Sun et al. 1991; Qiu and Xu 1992; Xu et al. 1994; Laroche and Zawadzki 1994). A variational data analysis method easily combines all the information contained in both the reflectivity and the radial velocity observations to retrieve the best horizontal wind field. This capability will be demonstrated in this paper by using the conservation of reflectivity and the momentum equation for the radial velocity as physical constraints. We also show that, within the variational method proposed here, it is possible to combine the ideas contained in both VVP and TREC.

Section 2 describes the four methods studied here for the retrieval of the horizontal steady-state wind

field from two or three time sequences of observations. The TREC method is first presented. Two methods similar to TREC, in which the difference between consecutive observations of reflectivity is minimized, are then described. The last method applies the weak constraint formulation proposed by Laroche and Zawadzki (1994) to the conservation of reflectivity and the momentum equations for radial velocity. All the methods are compared in section 3 using dual-Doppler data collected in the clear-air PBL during the Convection and Precipitation/Electrification (CaPE) Experiment. A series of experiments is described in section 4.

2. Description of the methods

a. Tracking radar echoes by correlation (TREC)

The TREC method was originally developed by Rinehart (1979) and then extended by Smythe and Zrnić (1983) and Tuttle and Foote (1990) for estimating the wind field from the motion of reflectivity patterns. In this method the wind vector $\mathbf{v} = (u, v)$ is assumed uniform over a domain containing a number S of reflectivity η values; $\mathbf{v}$ is determined by the space lag that maximizes the correlation function of η between two successive scans. This correlation is calculated using

$$R_{12} = \frac{\sum_{i=1}^{S} [\eta_2(\mathbf{r}_i) - \bar{\eta}_2][\eta_1(\mathbf{r}_i - \mathbf{v}\Delta t) - \bar{\eta}_1]}{\left\langle \left\{ \sum_{i=1}^{S} [\eta(\mathbf{r}_i) - \bar{\eta}_2]^2 \right\} \left\{ \sum_{i=1}^{S} [\eta(\mathbf{r}_i - \mathbf{v}\Delta t) - \bar{\eta}_1]^2 \right\} \right\rangle^{1/2}}, \quad (1)$$

where η_1 and η_2 represent reflectivity observations in the first and second scan, respectively; $\mathbf{r}_i$ is the two-dimensional gridpoint position, Δt is the time interval between the two scans, and the overbar denotes the spatial average of reflectivity over the domain S.

To find the maximum correlation, several values of R_{12} corresponding to various displacements $\mathbf{v}\Delta t$ are calculated. The greatest displacement is limited to a search radius $r = v_{\max}\Delta t$ where $v_{\max}$ is the maximum velocity expected. When the data are analyzed on a horizontal plane, with a regular grid point as in this study, the sector in the second scan is shifted successively by one gridpoint spacing in both the x and y directions. The maximum value of the cross correlation function is found by interpolation between the discrete gridpoint values (as in Tuttle and Foote 1990). This procedure is repeated over various areas of S grid points in order to construct the wind field in the domain of interest. It should be pointed out that the vectors $\mathbf{r}_i$ in (1) represent the displacement due to the wind only in clear air. When vertical advection is important, as in precipitation, echo motion on the horizontal plane does not reflect the wind field.

This method can easily be extended to consider three consecutive scans (or time levels). The correlation coefficient becomes

$$R_{123} = \frac{\sum_{i=1}^{S} [\eta_2(\mathbf{r}_i) - \bar{\eta}_2]\{[\eta_1(\mathbf{r}_i - \mathbf{v}\Delta t) - \bar{\eta}_{13}] + [\eta_3(\mathbf{r}_i + \mathbf{v}\Delta t) - \bar{\eta}_{13}]\}}{\left\langle \left\{ 2\sum_{i=1}^{S} [\eta_2(\mathbf{r}_i) - \bar{\eta}_2]^2 \right\} \left\{ \sum_{i=1}^{S} [\eta_1(\mathbf{r}_i - \mathbf{v}\Delta t) - \bar{\eta}_{13}]^2 + \sum_{i=1}^{S} [\eta_3(\mathbf{r}_i + \mathbf{v}\Delta t) - \bar{\eta}_{13}]^2 \right\} \right\rangle^{1/2}}, \quad (2)$$

where $\bar{\eta}_{13} = 0.5(\bar{\eta}_1 + \bar{\eta}_3)$.

In this case, the cross correlation of the second scan is performed backward with the first scan, and forward with the third scan. Hence, the estimated echo motion corresponds to the grid point located at the center of the area and it is representative of the motion at the time of the second scan. This represents an advantage with respect to TREC with two scans in which the velocity corresponds to intermediate grid points in time and space. On the other hand, TREC with three scans requires the conservation of the wind field to hold over a longer time period.

When the radial velocity is observed at low angular elevations (<5°) by a Doppler radar, the TREC method can be used to retrieve the tangential component of the wind only. In this case the radial component of the uniform horizontal wind can be given by the mean values of the observed radial velocity $\bar{v}_r$ over the sector. The tangential component is obtained by seeking the highest correlation along a line perpendicular to the radial direction. This line crosses the radial direction at a distance $\bar{v}_r\Delta t$ from the center of the sector. Thus, the derived tangential velocity does not necessarily correspond to the highest correlation

value but is found along a ridge in the correlation function.

b. *Tracking radar echoes by difference (TRED)*

We develop here two methods that conceptually link the TREC method with the variational method presented later. As in the TREC method, the wind field is estimated on subdomains or sectors, but the two-dimensional conservation of reflectivity is used explicitly as a constraint.

The two-dimensional conservation equation for reflectivity is defined as follows:

$$\frac{\partial \eta}{\partial t} + \frac{\partial u\eta}{\partial x} + \frac{\partial v\eta}{\partial y} = S_\eta. \tag{3}$$

In the absence of sources or sinks S_η, and when the compressibility term $(\eta \partial u/\partial x + \eta \partial v/\partial y)$ is negligible, the two-dimensional conservation equation for reflectivity becomes

$$\frac{d\eta}{dt} = \frac{\partial \eta}{\partial t} + u\frac{\partial \eta}{\partial x} + v\frac{\partial \eta}{\partial y} = 0. \tag{4}$$

This relation will be referred to as the η-conservation equation. Using the upstream semi-Lagrangian scheme, the conservation equation for reflectivity becomes

$$\eta_2(\mathbf{r}) - \eta_1(\mathbf{r} - \mathbf{v}\Delta t) = 0. \tag{5}$$

All symbols have the same meaning as in (1). The retrieved wind vector $\mathbf{v} = (u, v)$ can be obtained by minimizing the residual of (5) over each grid point in the least-squares sense; that is,

$$[\eta_2(\mathbf{r}) - \eta_1(\mathbf{r} - \mathbf{v}\Delta t)]^2. \tag{6}$$

If we suppose that S reflectivity values of an entire area move at the same velocity, the uniform wind for this area can be obtained by finding the minimum of the following cost function:

$$J_{12} = \sum_{i=1}^{S} [\eta_2(\mathbf{r}_i) - \eta_1(\mathbf{r}_i - \mathbf{v}\Delta t)]^2. \tag{7}$$

This assumption on the wind field in the sector defined by the S reflectivity values can be seen as a "strong" smoothness constraint since no variation in the local wind field is allowed. Thus, two constraints (the conservation of reflectivity and the uniform wind structure in the sector) are actually included in the cost function. Expression (7) also indicates that, in fact, $\mathbf{v} = (u, v)$ is found by minimizing the difference between η_1 and η_2. If the reflectivity field does not change during Δt, then finding the minimum between η_1 and η_2 is equivalent to maximizing its cross correlation with the TREC method and should lead to the same results. In effect, after a few algebraic manipulations, (1) and (7) can be written as follows:

$$R_{12} = a \sum_{i=1}^{S} \eta_2(\mathbf{r}_i)\eta_1(\mathbf{r}_i - \mathbf{v}\Delta t) + b,$$

$$J_{12} = -2 \sum_{i=1}^{S} \eta_2(\mathbf{r}_i)\eta_1(\mathbf{r}_i - \mathbf{v}\Delta t) + c,$$

where

$$a = \{S[\overline{\eta_1^2} - (\bar{\eta}_1)^2][\overline{\eta_2^2} - (\bar{\eta}_2)^2]\}^{-1/2},$$

$$b = -2a\bar{\eta}_1\bar{\eta}_2,$$

$$c = S(\bar{\eta}_1^2 + \bar{\eta}_2^2).$$

As long as the coefficients a, b, and c remain constant for any displacement $\mathbf{v}\Delta t$, we can see that minimizing $-2 \sum \eta_1\eta_2$ is equivalent to maximizing $a \sum \eta_1\eta_2$. The coefficients remain constant only if $\overline{\eta_1}$ and $\overline{\eta_1^2}$ remain constant when the sector is shifted in the first scan. However, we will see that this is not necessarily the case with actual radar data where the reflectivity field is deformed by the nonuniform wind field and modified by the source–sink terms in the successive scans.

TRED can also be extended to three time levels as in the TREC method with

$$J_{123} = \sum_{i=1}^{S} [\eta_2(\mathbf{r}_i) - \eta_1(\mathbf{r}_i - \mathbf{v}\Delta t)]^2 + [\eta_3(\mathbf{r}_i + \mathbf{v}\Delta t) - \eta_2(\mathbf{r}_i)]^2. \tag{8}$$

The minimum can be found in the same way as with TREC by calculating several values of J_{12} (or J_{123}) corresponding to various displacements $\mathbf{v}\Delta t$.

c. *Variational echo tracking (VET)*

As an alternative to the minimization procedure described above, the minimum in the cost function can be found by optimization methods such as described by Navon and Legler (1987). The components of the wind vector (u, v) corresponding to the minimum of the cost function are found by iteration with

$$\mathbb{X}_{k+1} = \mathbb{X}_k + \alpha_k \mathbb{d}_k, \tag{9}$$

where $\mathbb{X}_k$ is a vector containing the control variables [that is, (u, v) in our problem], $\mathbb{d}_k$ is a search direction calculated from the gradient of the cost function with respect to the control variables, α_k is an optimal step length, and k is the iteration number. The method requires a first guess of the control variables in $\mathbb{X}_0$. In this method, a first guess equal to zero is chosen for most experiments presented in section 4. Here $\mathbb{d}_k$ and α_k are calculated with the conjugate-gradient method (Powell 1977).

For J_{12}, the gradient components of the cost function, with respect to (u, v), are simply

$$\frac{\partial J_{12}}{\partial u} = 2\Delta t \sum_{i=1}^{S} [\eta_2(\mathbf{r}_i) - \eta_1(\mathbf{r}_i - \mathbf{v}\Delta t)] \frac{\partial \eta_1(\mathbf{r}_i - \mathbf{v}\Delta t)}{\partial x}; \tag{10a}$$

$$\frac{\partial J_{12}}{\partial v} = 2\Delta t \sum_{i=1}^{S} [\eta_2(\mathbf{r}_i) - \eta_1(\mathbf{r}_i - \mathbf{v}\Delta t)] \frac{\partial \eta_1(\mathbf{r}_i - \mathbf{v}\Delta t)}{\partial y}. \tag{10b}$$

A bilinear interpolation scheme is used to calculate η_1 as well as its gradient at $\mathbf{r}_i - \mathbf{v}\Delta t$. Similar expressions are obtained for J_{123}. All the experiments that use this minimization procedure will be referred to as the variational echo tracking (VET) method.

Since J_{12} and J_{123} depend on only two variables (u and v), it is possible to visualize the cost functions and its secondary minima if some exist. This will be very useful for studying the behavior of the minimization methods. To construct the whole wind field, each wind vector can be retrieved individually by applying the method on several sectors in the domain. However, all the wind components can also be retrieved simultaneously using a global minimization. In this case, **X** contains all the horizontal wind components and the cost function is the sum of all J_{12} (or J_{123}) in the domain.

When the radial velocity is also observed at low angular elevations, the tangential velocity can be retrieved by seeking the minimum of the cost function along a line perpendicular to the radial direction, as described in the previous section for the TREC method. An alternate procedure is to minimize the squared difference between the radial component for the retrieved uniform wind and the corresponding observed radial velocity in the sector. This can be done by adding the following term to the cost function:

$$\beta \sum_{i=1}^{S} (v_{ri} - \tilde{v}_{ri})^2, \tag{11}$$

where β is a constant weight, v_{ri} is the radial component of the retrieved wind vector defined by $v_{ri} = u \cos\theta_i + v \sin\theta_i$, θ_i is the angle of the grid point i from the radar site (see Fig. 1), and $\tilde{v}_{ri}$ is the corresponding observed radial velocity averaged over two or three time levels. In this case, the observed radial velocity field is used as weak constraint; the retrieved radial velocities will not be exactly equal to the observed values, thus allowing for measurement errors in v_r.

It is interesting to note that this constraint is also used in the VVP method when employed to estimate a uniform wind over a given sector (Doviak and Zrnić 1993). In VVP, the uniform wind is obtained by minimizing (11) with the least-squares fit method. A unique solution is found because the radial and tangential components of the uniform wind at the center of the sector, v_{rc} and $v_{\theta c}$, are related through

$$v_{ri} = v_{rc} \cos\Delta\theta + v_{\theta c} \sin\Delta\theta, \tag{12}$$

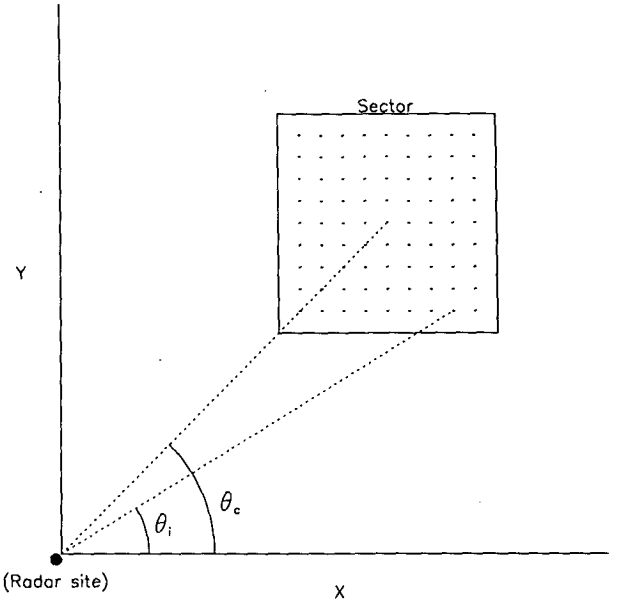

FIG. 1. Schematic showing the angular distances θ_i and θ_c with respect to the radar site.

where $\Delta\theta = \theta_c - \theta_i$, and θ_c is the angular coordinate of the center of the sector (Fig. 1). When $\Delta\theta$ is small for all the grid points in the sector, the second term on the right-hand side of (12) becomes negligible and only the term that includes v_{rc} contributes to the constraint. In other words, for sectors with a small angular extent, the tangential component of the uniform wind is not well determined by (11). This explains why the VVP method requires a wide azimuthal sector (>30°) to estimate the uniform wind field with sufficient accuracy as demonstrated by Doviak and Zrnić (1993).

Thus, when (11) is added to the cost function (7) or (8), we combine the constraints used in the TREC method with those of the VVP method. Contrary to VVP, large sectors are not necessarily required since two independent constraints (or sources of information) are used simultaneously and each may contribute to the retrieval according to its capability. The constant weight β controls the relative importance of each constraint. However, it should be mentioned that VVP uses only one time level while in our method $S > 1$ and the wind is assumed constant in the time interval. That is, besides the fact that two sources of information are combined in our retrieval we are trading-off the VVP assumption of uniformity over large sectors for the assumption of uniformity over small sectors *and* uniformity in the time interval.

d. Variational retrieval of the horizontal wind field

In the previous section, the conservation of reflectivity and uniform wind were used as constraints, as an approximation to the evolution of the observed re-

flectivity field. A variational formulation can combine these constraints, as well as additional ones, into a single algorithm. Following the weak formulation described by Laroche and Zawadzki (1994), the wind field can be retrieved from the η-conservation equation by minimizing the following cost function:

$$J_\eta = k_\eta \sum_{n=0}^{N-1} \tilde{\epsilon}_{\eta n}^{\mathrm{T}} \tilde{\epsilon}_{\eta n}, \tag{13}$$

where k_η is constant weights, $\tilde{\epsilon}_{\eta n}$ is a vector containing the residuals of the η-conservation equation in the domain, T stands for the vector transpose, and N is the number of consecutive scans. A centered semi-Lagrangian scheme is used to define the residuals:

$$\tilde{\epsilon}_{\eta n} = \left[\frac{\eta(\mathbf{r} + \alpha/2)_{n+1} - \eta(\mathbf{r} - \alpha/2)_n}{\Delta t} \right], \tag{14}$$

where vectors $\eta(\mathbf{r} + \alpha/2)_{n+1}$ and $\eta(\mathbf{r} - \alpha/2)_n$ contain the interpolated reflectivity observations at time step $n + 1$ and n, respectively, $\mathbf{r}$ contains the gridpoint coordinates, and α is the two-dimensional displacement $\mathbf{v}\Delta t$.

Since the radial velocity field is also observed in time, the momentum equation for the radial velocity can also be used as a constraint. In the horizontal plane, this equation is defined by

$$\frac{dv_r}{dt} - \frac{v_\theta^2}{r} = -\frac{1}{\rho}\frac{\partial p}{\partial r} + F_t, \tag{15}$$

where r is the radial distance from the radar site, p is the pressure, ρ is the density, F_t is a dissipation term, and v_θ is the tangential velocity. If we partition the wind into its steady state (u, v, $v_{\theta s}$) and temporal fluctuation (u', v', v'_θ) components, (15) becomes

$$\frac{\partial v_r}{\partial t} + u\frac{\partial v_r}{\partial x} + v\frac{\partial v_r}{\partial y} - \frac{v_{\theta s}^2}{r} = -u'\frac{\partial v_r}{\partial x} - v'\frac{\partial v_r}{\partial y} + \frac{2v_{\theta s}v'_\theta}{r} - \frac{1}{\rho}\frac{\partial p}{\partial r} + F_t, \tag{16}$$

where products of temporal fluctuation (considered small) are neglected. The last two terms on the right-hand side can be seen as sources or sinks of this equation. These terms are unknown, which may limit the use of this equation as a constraint. However, when the advection is the dominant term, the residual of left-hand side can be minimized to retrieve the steady-state part of the wind field. The left-hand side of (16) will henceforth be referred to as the r-momentum equation. As in the η-conservation equation, the r-momentum equation can be used to retrieve the horizontal wind field by minimizing the following expression:

$$J_m = k_m \sum_{n=0}^{N-1} \tilde{\epsilon}_{mn}^{\mathrm{T}} \tilde{\epsilon}_{mn}, \tag{17}$$

where k_m is constant weight and the residual $\tilde{\epsilon}_{mn}$ is defined by the following vector:

$$\tilde{\epsilon}_{mn} = \left[\frac{\tilde{\mathbf{v}}_r(\mathbf{r} + \alpha/2)_{n+1} - \tilde{\mathbf{v}}_r(\mathbf{r} - \alpha/2)_n}{\Delta t} - \frac{\mathbf{v}_{\theta n}^2}{r} \right], \tag{18}$$

where $\tilde{\mathbf{v}}_r(\mathbf{r} + \alpha/2)_{n+1}$ and $\tilde{\mathbf{v}}_r(\mathbf{r} - \alpha/2)_n$ contain the interpolated radial velocity observations at time step $n + 1$ and n, respectively, with all other symbols being as in (14). This constraint can be used only if the radial velocities are observed at low angular elevations (<5°). Otherwise, the spherical form of (15) should be used.

The wind field can be retrieved such that its radial component at a given grid point is as close as possible to that observed during the N consecutive scans. This can be done by minimizing the following expression:

$$J_v = k_v \sum_{n=0}^{N} (\mathbf{v}_r - \tilde{\mathbf{v}}_{rn})^{\mathrm{T}} (\mathbf{v}_r - \tilde{\mathbf{v}}_{rn}), \tag{19}$$

where $\mathbf{v}_r$ is a vector containing all the radial components of the wind field, defined at a given grid point i by $v_{ri} = u_i \cos\theta_i + v_i \sin\theta_i$, and $\tilde{\mathbf{v}}_{rn}$ contains the corresponding observations at time step n.

Finally, a smoothness penalty function can be applied to prevent the retrieved wind field from being too noisy. There exists several forms of two-dimensional smoothness constraints (Thacker 1988). We use here the one suggested by Wahba and Wendelberger (1980), given by

$$J_2(u) = \gamma \int\int_{x,y} \left(\frac{\partial^2 u}{\partial x^2} \right)^2 + 2\left(\frac{\partial^2 u}{\partial x \partial y} \right)^2 + \left(\frac{\partial^2 u}{\partial y^2} \right)^2 dxdy, \tag{20}$$

where γ is a constant weight. This expression is discretized by using finite-difference methods. A similar expression is defined for the v component. This constraint is less restrictive than the uniform wind assumption used in the three methods previously described. It allows the control of the effective resolution of the retrieval, as we will see later on.

All the constraints described above form an overdetermined system. Indeed, the constraint defined either by J_η or J_m is sufficient to retrieve the wind field from a time series of observed reflectivity or radial velocity fields, as long as the fields are not homogeneous and the evolution of the perturbations can be approximated by the model equation (Qiu and Xu 1992). However, the retrieval can be strongly affected by the observational and model errors. Since both constraints can provide independent information on the wind field, the sum of J_η and J_m is likely to give a more stable solution. The stability and accuracy of the retrieval can further be improved by adding the last two constraints defined by J_v and J_2. Therefore, with all constraints together, the retrieved horizontal wind field can be estimated by minimizing the following cost function

$$J_{2D} = J_\eta + J_m + J_v + J_2(u) + J_2(v). \tag{21}$$

An optimal solution can be found only if the weights k_η, k_m, k_v, and γ are properly chosen. The first three

weights should reflect the precision of the equations and of the data, while the last one controls the desired degree of smoothness of the retrieved wind. The observational errors are typically 1 dBZ for the reflectivity and 1 m s^{-1} for the radial velocity. However, the model errors are difficult to determine because they are case dependent. These errors depends on how well the equations can represent the phenomenon observed. Since the complexity of Doppler radar observations changes in space and in time, the structure of the model errors is variable and not homogenous (as we will see later). Therefore, the method proposed in this section is valuable only if the retrieval is relatively insensitive to the choice of the weights. This can be assessed by retrieving the wind field with various set of weights. The variability of the results indicates the degree of sensitivity as demonstrated in the next section.

The minimization of the cost function (21) is performed with the following algorithm:

1) Make a first guess $\mathbf{X}_0$ of the horizontal wind field ($\mathbf{X}_0$ is set to zero in most experiments presented in this work);

2) Calculate the cost function and its gradient with respect to the control variables (i.e., the horizontal wind field) to calculate the search direction $\mathbf{d}_k$;

3) Calculate the improved guess $\mathbf{X}_{k+1} = \mathbf{X}_k + \alpha_k \mathbf{d}_k$ with the conjugate gradient method (k is the iteration number); and

4) Exit if an acceptable reduction in the gradient of the cost function is achieved at a given number of iterations; otherwise, return to step 2 for another iteration.

3. The CaPE data

The CaPE experiment was conducted during the summer of 1991 in east-central Florida (Gray 1991). On 11 August 1991 two C-band Doppler radars (CP-3 and CP-4) were used to observe a sea-breeze front. The relative positions of the radars and the observed region are shown in Fig. 2. Three successive scans between 2019:49 and 2026:37 UTC were analyzed.

Data from the CP-3 radar are used in all single-Doppler retrieval experiments presented in the next section. Observations from the CP-4 radar are used only in the dual-Doppler wind analysis. Reflectivity and radial velocity observations are analyzed in a domain of 25 km × 25 km (thick box in Fig. 2) at a height of 600 m AGL. The gridpoint spacing is 250 m in both directions. Observations at grid points are interpolated by using an exponential weighting function with a radius of influence R_i = 200 m (Barnes 1964).

The analyzed reflectivity fields for the three time sequences are shown in Fig. 3. The highest radar elevation in the domain is 2.0°. Thus, the assumption that the radial velocity corresponds to one component of the horizontal wind field is valid. The wind field is

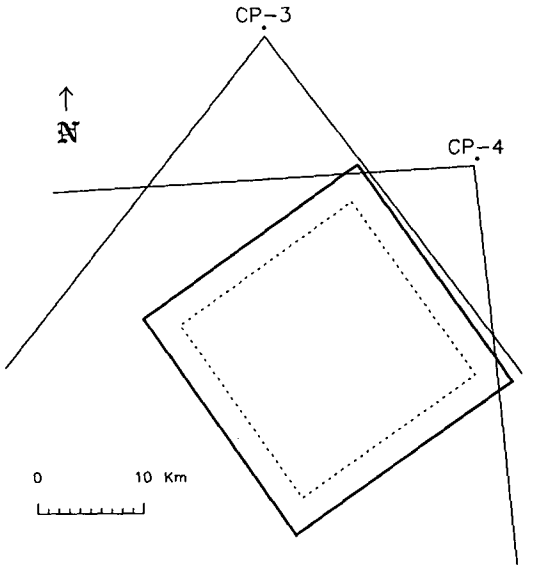

FIG. 2. Map showing radar locations relative to the analysis domain (thick box) and the retrieval domain (thin box) considered in this study.

retrieved in the inner domain D1 of 20 km × 20 km to allow tracking or interpolation of data outside the retrieval domain. Most of the echoes are from clear air except in a small precipitating cell (identified as such by its large vertical extent) located in the smaller domain D2. The maximum reflectivity values in this cell are near 35 dBZ corresponding to a light shower. Figure 3 shows that this cell is moving away from the sea-breeze front during the three sequences. We should expect a poor performance of retrievals based on two-dimensional echo tracking in the D2 region.

Although the reflectivity fields are only a few minutes apart, the local changes in the pattern are significant even outside D2. In fact, these changes appear to be more chaotic than the changes often observed in precipitation during comparable time intervals. This suggests that advection is not the only cause of the change in the pattern. The sources and sinks of clear air reflectivity, very likely related to turbulent processes, play an important role. This sets severe limits to the assumption of conservation of reflectivity underlying all the retrieval methods described above.

Figure 4 shows the high-resolution dual-Doppler wind field analysis at 2022:24 UTC. The airflow is very weak (less than 5 m s^{-1}), which is favorable for sea-breeze development. This wind field represents a good first test bed for the intercomparison of methods.

4. Retrieval experiments

The performance of all retrievals will be evaluated by the root-mean-square difference (rmsd) between the retrieved tangential wind component (the unobserved

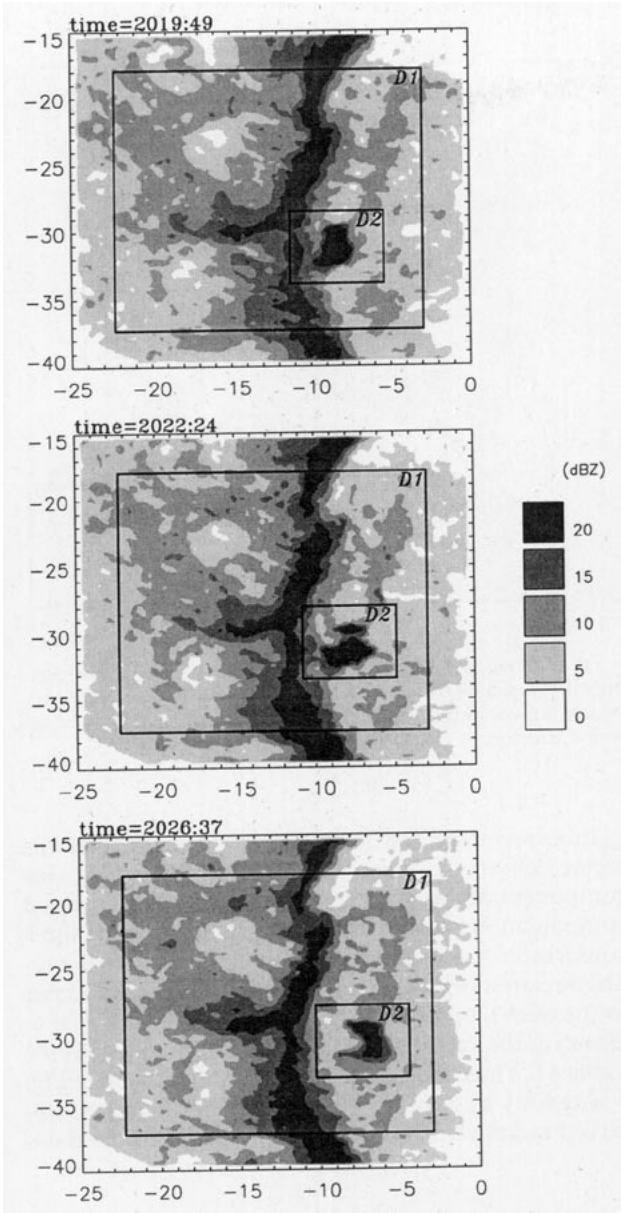

FIG. 3. Reflectivity fields observed at a constant height of 600 m AGL by the CP-3 radar for the three time sequences used in this study (UTC). In all experiments, the wind field is retrieved in subdomain D1. Domain D2 delimits a precipitating cloud. The horizontal coordinates (km) are referenced to the CP-3 radar site.

wind component by the CP-3 radar) and the corresponding wind component obtained from dual-Doppler analysis:

$$\mathrm{rmsd}(v_\theta) = \left\{ \frac{1}{M} \sum_{1}^{M} [(v_\theta)_{\mathrm{ret}} - (\bar{v}_\theta)_{\mathrm{dual}}]^2 \right\}^{1/2}, \quad (22)$$

where M is the number of wind vectors in the domain. Since each wind vector is retrieved on individual sectors in the TREC, TRED, and VET methods, $(\bar{v}_\theta)_{\mathrm{dual}}$ is obtained from the mean dual-Doppler wind vector over the corresponding sector.

a. *Intercomparison of TREC, TRED, and VET methods*

Ten experiments using TREC, TRED, and VET methods are summarized in Table 1. The purpose of the first seven experiments is to the compare TREC and TRED for two resolution areas over which the wind is assumed uniform and using two or three scans. In the first two experiments, two scans (2019:49 and 2022:24 UTC) and resolution areas of 2 km × 2 km, containing $N = 64$ reflectivity values, are employed. Results for TREC are shown in Fig. 5. The retrieved wind field (thick vectors) looks rather noisy compared with the wind field derived from dual-Doppler analysis (thin vectors). Moreover, several echo motions (indicated by thick crosses) are rejected because the highest correlation is found for unrealistically large lags. This can be explained by the fact that the reflectivity patterns within areas of 2 km × 2 km are too incoherent to be tracked correctly between two consecutive scans. Similar results are obtained with TRED in experiment 2.

Results for TREC improve when three scans are used (experiment 3), as shown in Fig. 6. However, the rmsd(v_θ) degrades from 1.47 m s^{-1} in experiment 2 to 1.91 m s^{-1} when three scans are used with TRED. The more stringent steady wind assumption over three scans cannot explain this degradation because it would affect also TREC. On the other hand, the statistical fluctu-

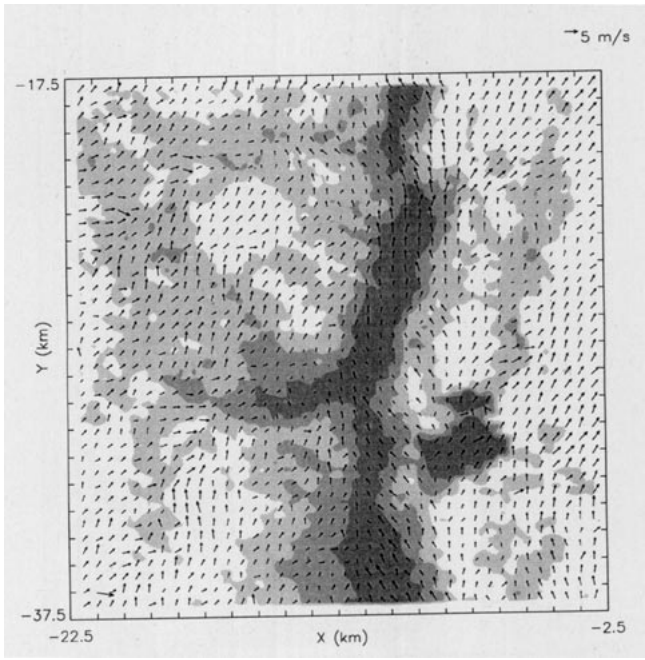

FIG. 4. Dual-Doppler wind field analysis at $z = 600$ m and at 2022:24 UTC. The grid spacing is 250 m in both directions, but wind vectors appear at every 500 m for clarity. The background is the reflectivity field at the same altitude and time.

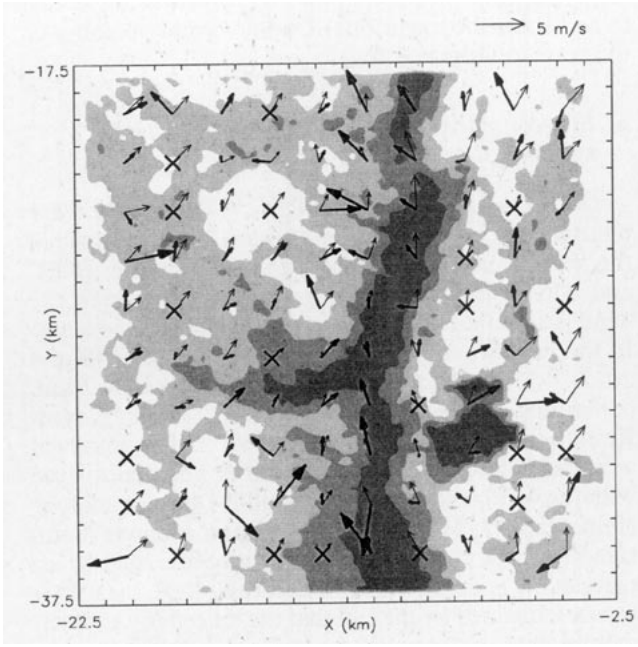

FIG. 5. Retrieved wind field (thick vectors) obtained with the TREC method using two time levels (2019:49 and 2022:24 UTC) and mean dual-Doppler winds (thin vectors) over arrays of 2 km × 2 km. The background is the reflectivity field at 2022:24 UTC as shown in Fig. 3.

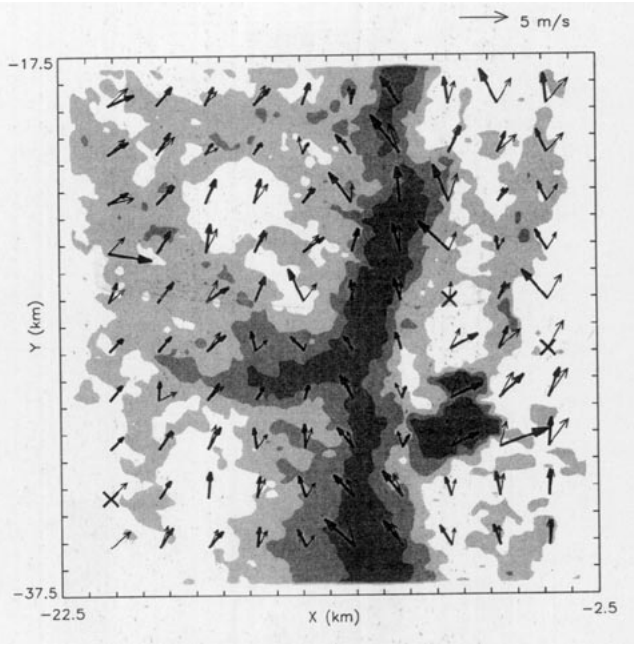

FIG. 7. Same as in Fig. 6 but the TREC method is used to retrieve only the tangential component of the wind vectors. The radial component is given by the mean value of the observed Doppler velocities over the sectors.

ations of rmsd(v_θ) due to the limited number of samples M (≤ 100) could be responsible for the degradation. That is, the result with two scans can, by chance, be better than the one obtained with three scans.

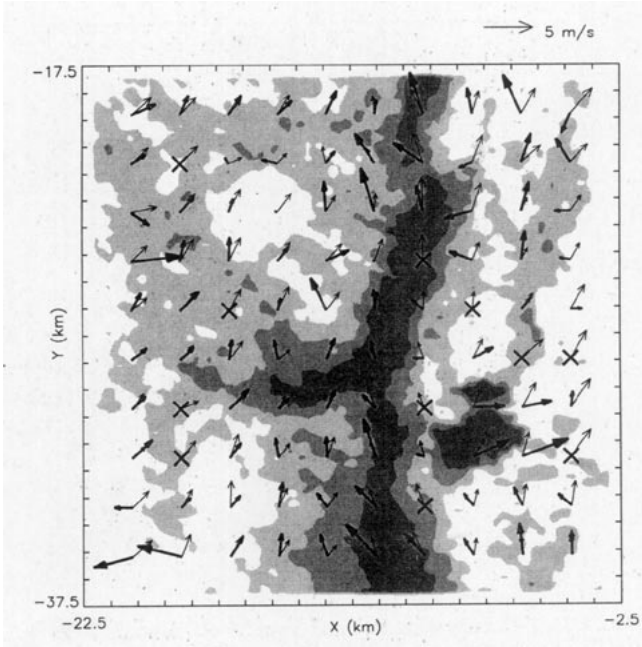

FIG. 6. Same as in Fig. 5 but for three time levels (2019:49, 2022:24, and 2026:36 UTC).

In experiment 5 with TREC, the mean (over the sector) observed radial velocity is employed as one component of the wind vector and only the tangential component is found by tracking echoes over the three consecutive scans along a line perpendicular to the radial direction (Fig. 7). This retrieved wind field is closer to the dual-Doppler wind analysis than that of Fig. 6. However the rmsd(v_θ) is not significantly reduced (see Table 1). Thus, the apparent improvement seen in Fig. 7 is mainly due to the introduction of the mean observed radial velocity, which is also used in the dual-

TABLE 1. Summary of experiments with TREC, TRED, and VET methods, ρ is the correlation between the retrieved and dual-Doppler tangential velocities.

Experiment	Time level	Sector (km^2)	rmsd (v_θ) (m s^{-1})	ρ
1 TREC	2	4	2.01	0.28
2 TRED	2	4	1.47	0.41
3 TREC	3	4	1.75	0.43
4 TRED	3	4	1.91	0.35
5 TREC (only on the tangential component)	3	4	1.64	0.42
6 TREC	3	16	1.16	0.64
7 TRED	3	16	1.23	0.70
8 VET	3	16	1.28	0.63
9 VET [as experiment 8 but with (11) added in J_{123}]	3	16	1.10	0.63
10 VET (as experiment 9 but on smaller sectors)	3	4	1.32	0.56

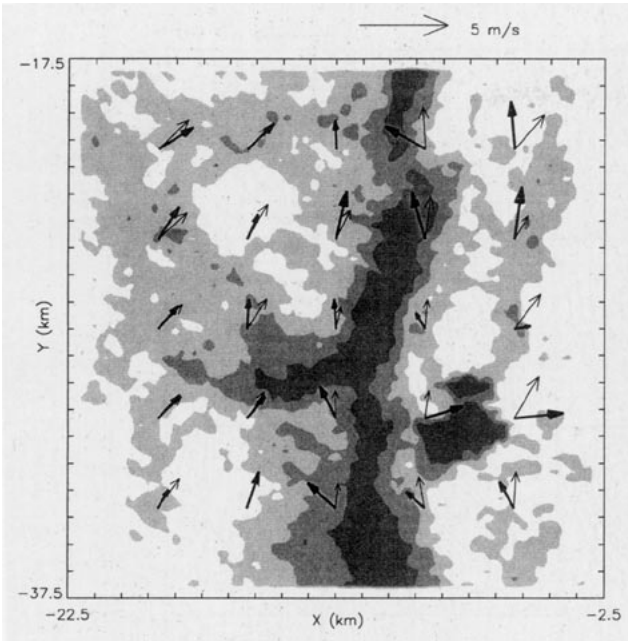

FIG. 8. Same as in Fig. 6 but using sectors of 4 km × 4 km.

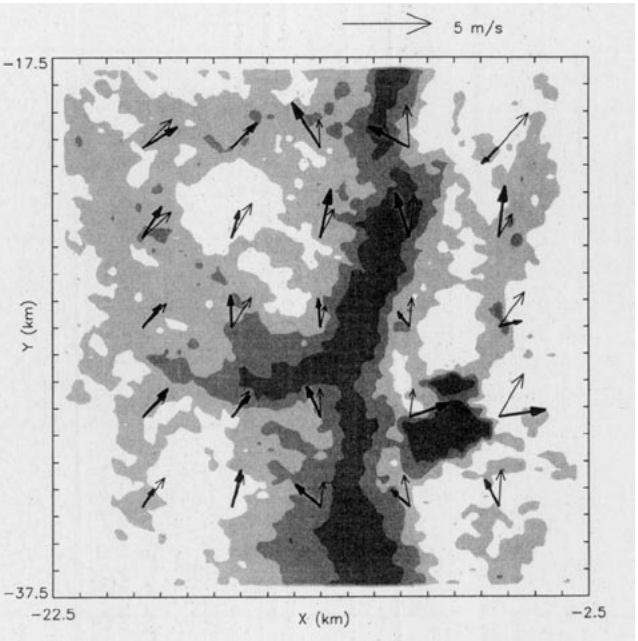

FIG. 9. Retrieved wind field (thick vectors) obtained with the TRED method using three time levels (2019:49, 2022:24, and 2026:36 UTC) and mean dual-Doppler winds (thin vectors) over arrays of 4 km × 4 km.

Doppler analysis. The echo tracking along only the tangential direction does not improve the retrieved tangential wind component.

To obtain a more stable solution, we enlarged the areas from 4 to 16 km^2 ($N = 256$ reflectivity values) in experiments 6 and 7. Three time levels are used for this and of all the remaining experiments. The observed radial velocity is not included in these experiments. Figure 8 shows results obtained with TREC. As expected no wind vector is rejected and the rmsd(V_θ) decreases from 1.75 to 1.16 m s^{-1}. As shown in Fig. 9 a similar improvement of overall quality of retrieval is obtained with TRED, although the individual wind vectors differ in Figs. 8 and 9. These differences are due to the variation of the mean and of the squared mean of η_1 and η_3 over the sectors for different lags $\mathbf{v}\Delta t$, as discussed in section 2b. The two vectors in the southeast represent the displacement of the rain cell away from the sea-breeze front and thus should not be interpreted as wind vectors.

In experiment 8, the VET method is employed to retrieve the horizontal wind field (Fig. 10). As in the two previous experiments, areas of 4 km × 4 km and three time sequences are used. The method is very efficient since from a first guess set to zero, only five iterations or less are necessary to reach the minimum of the cost function (8) for each wind vector. We see that the results in Figs. 10 and 9 are comparable. Most vectors are similar but a few are quite different, particularly in the wind vector indicated by P (which is close to zero in Fig. 10).

To better understand these differences, let us examine the topology of the cost functions at all grid points. Figure 11 displays these normalized cost functions; thick vectors are the retrieved velocities obtained with VET while the thin vectors represent the dual-Doppler winds. Positions of the absolute minima are given by the stars. We can see that the pattern of the cost function varies from point to

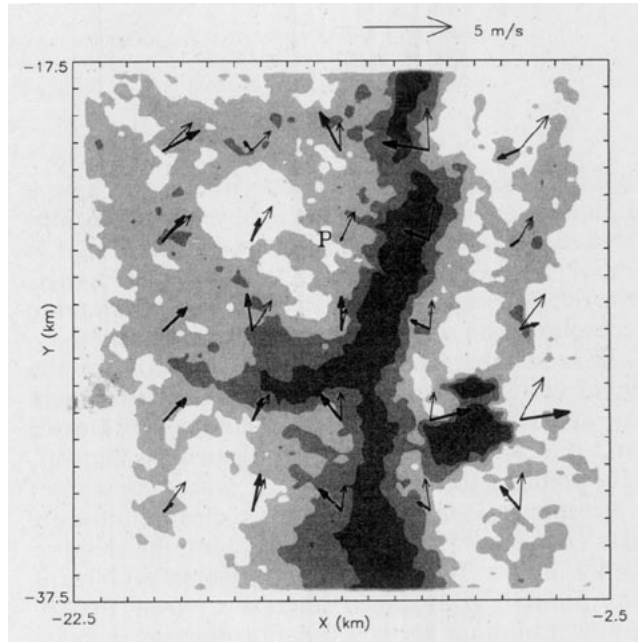

FIG. 10. Same as in Fig. 9 but using the VET method.

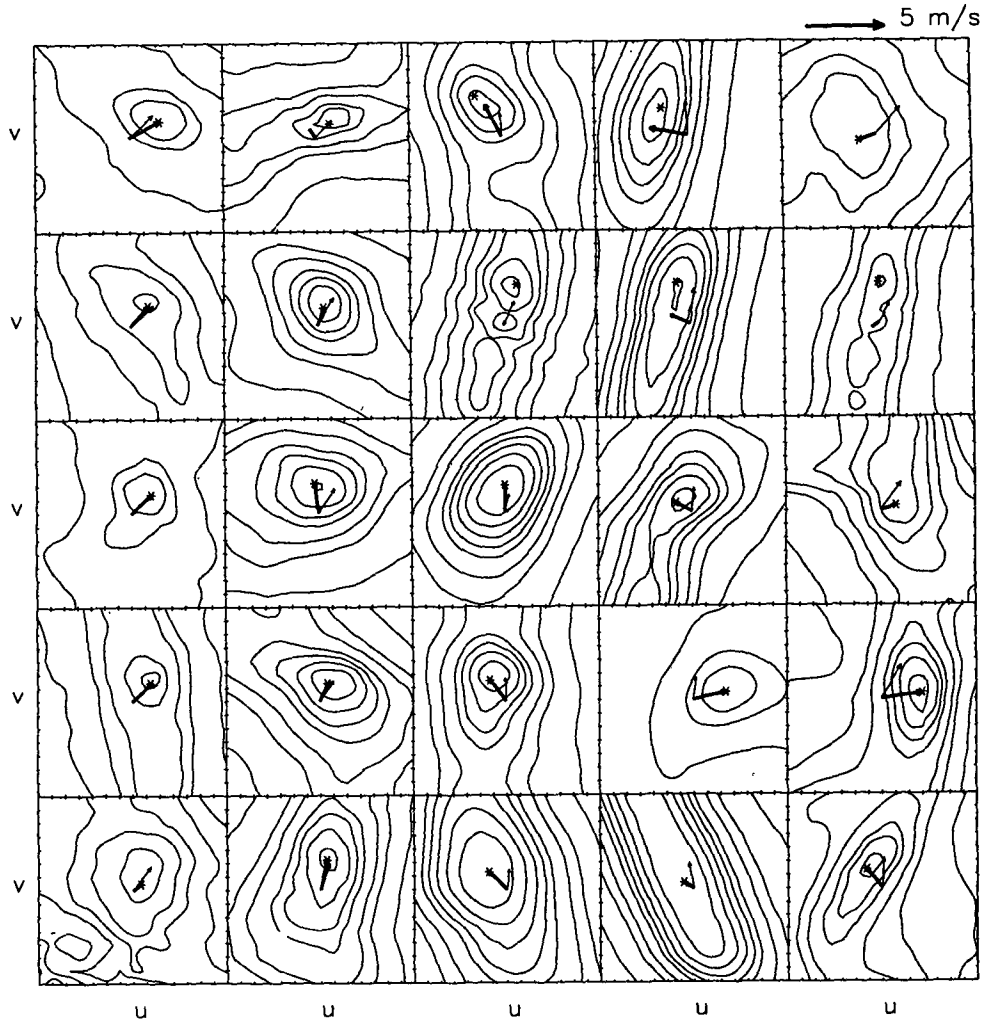

FIG. 11. Fields of normalized J_{123} for each analyzed wind vector shown in Fig. 10 as a function of u and v. The retrieved wind field from VET and the dual-Doppler wind field are represented by thick and thin vectors, respectively. The asterisks indicate the absolute minimum positions of the cost functions.

point: some patterns are almost circular and have a unique minimum while others have multiple minima. Even in the subareas where the minimum is unique and well defined, as in the lower right corner, the retrieval can be poor. The situation is even more complex when multiple minima are present. Figure 12a shows the details of the cost function for the wind vector at grid point P. We can see that there are at least three local minima, indicated by crosses and one absolute minimum indicated by the star. The wind vector found with VET (the thick arrow) corresponds to the local minimum closest to the origin ($u = 0, v = 0$). For this grid point, the solution is not unique. It seems that our retrieval problem is not properly constrained since, away from the absolute minimum, the cost function does not increase continuously.

The retrieval by VET can further be constrained by adding the squared difference between the radial component of the derived uniform wind and the corresponding observed average radial velocity in the sector [i.e., expression (11)]. Figures 12b and 12c show the normalized cost function when (11) is added in J_{123} with β equal to 1.0 and 10.0, respectively. We can see the effect of this constraint as its weight increases. When $\beta = 1.0$, the constraint is weak compared to the conservation of reflectivity. There are still secondary minima but not at the same positions as in Fig. 12a. When $\beta = 10.0$, the constraint (11) becomes dominant and the shape of the cost function changes significantly to be almost quadratic. Figure 12c shows that the cost function is well conditioned and contains a unique minimum. This is also the case for all the cost function depicted in Fig. 11. When β is further increased, the

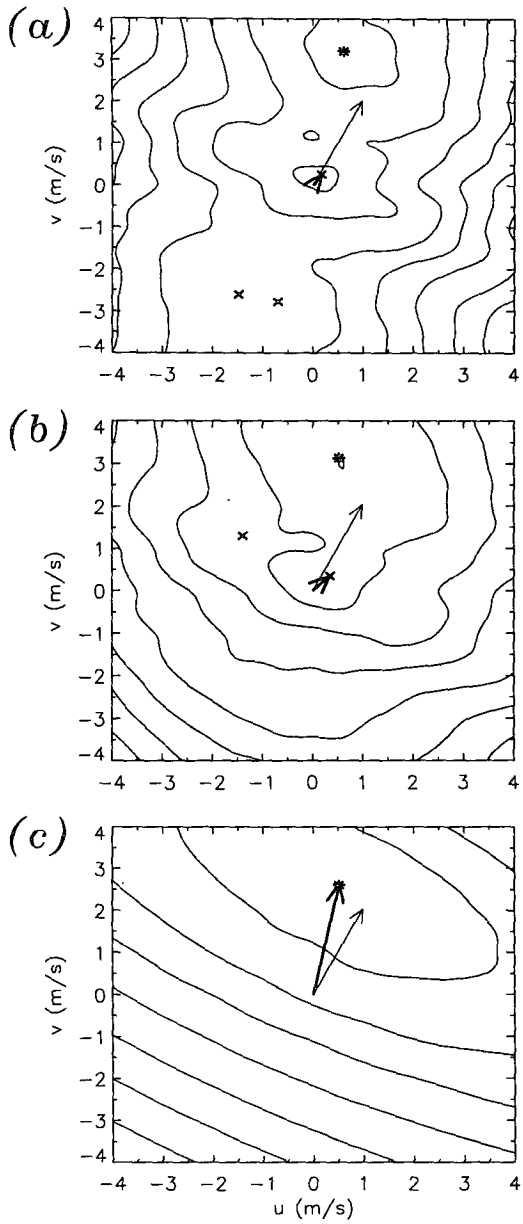

FIG. 12. Fields of normalized J_{123} for the wind vector indicated by P in Fig. 10 as a function of u and v when (a) $\beta = 0.0$, (b) $\beta = 1.0$, and (c) $\beta = 10.0$. The thick vector is the wind vector obtained with the VET method while the dual-Doppler wind is represented by the thin vector. Crosses indicate the secondary minima while the asterisks indicate the absolute minima.

cost function becomes strongly stretched along the axis perpendicular to the radial direction relative to the radar and the rate of convergence decreases when a global minimization is used to retrieve all the wind vector simultaneously in the domain.

The best retrieval on sectors of 4 km × 4 km is obtained with $\beta = 10.0$ as shown in Fig. 13 (experiment 9). The main improvement comes from the fact that the radial component of the retrieved wind field is constrained to be as close as possible to the observed radial velocity. Nevertheless, the rmsd(v_θ) is also improved compared with the previous experiment. The improvement in the rmsd(v_θ) is due to a better conditioning of the cost function as illustrated in Fig. 12c for the grid point P.

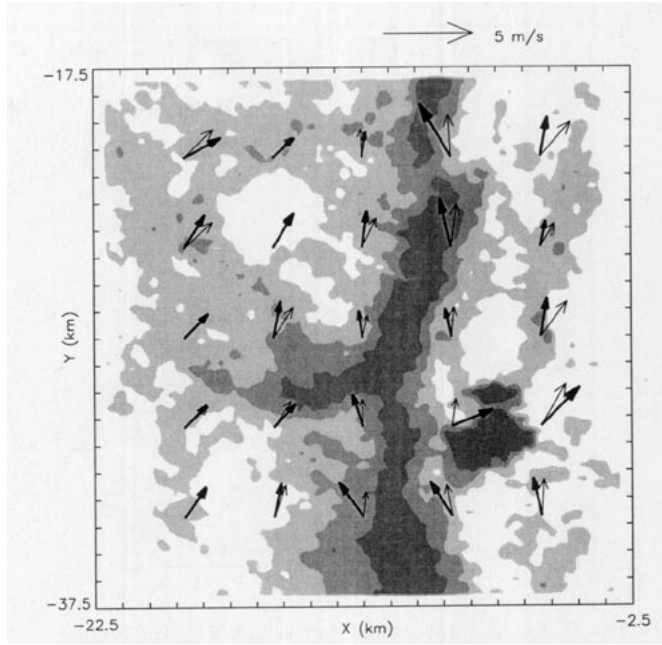

FIG. 13. Retrieved wind field on arrays of 4 km × 4 km by the VET method (thick vectors) when constraint Eq. (11) is added to the cost function with $\beta = 10.0$. The corresponding dual-Doppler wind field is depicted by thin vectors.

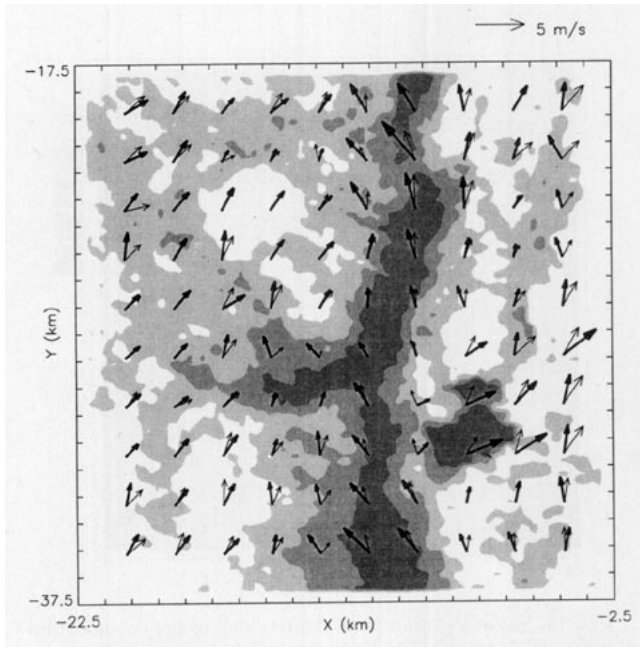

FIG. 14. Same as in Fig. 13 but the wind field is retrieved on arrays of 4 km × 4 km.

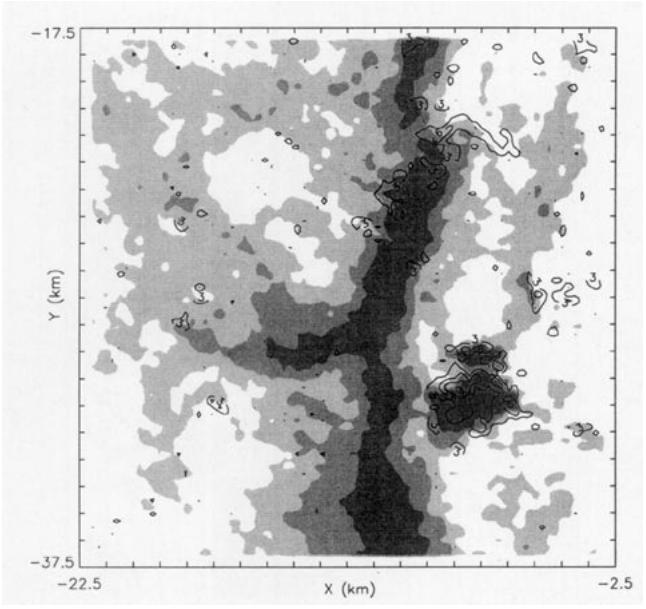

FIG. 15. Spatial distribution of the residuals of the conservation equation for reflectivity (10^{-2} dBZ s^{-1}).

In experiment (10), VET is used to retrieve the wind field on subareas of 2 km × 2 km, with both the conservation of reflectivity and the radial velocities differences ($\beta = 10.0$) as constraints. With these small areas, both TREC and TRED gave unsatisfactory wind fields (see Figs. 6 and 7 for TREC). The retrieval is improved when VET is used with the same number of scans. Figure 14 shows the retrieved wind field obtained by a global minimization with 30 iterations. The rmsd(v_θ)

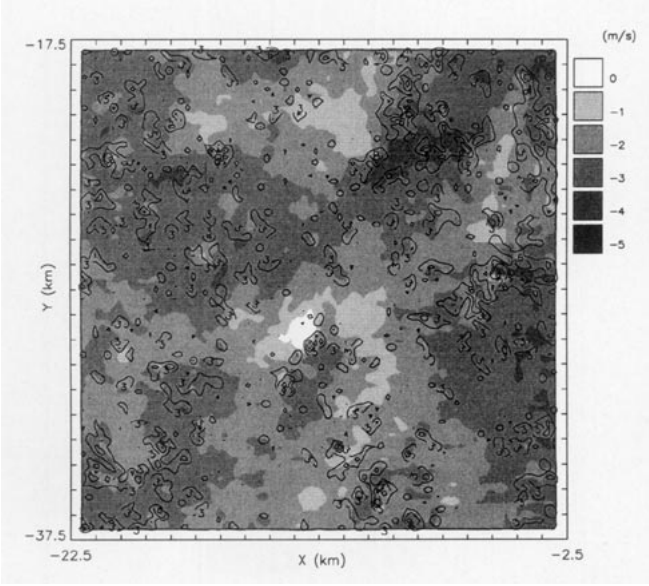

FIG. 16. Spatial distribution of the residuals of the r-momentum equation (10^{-3} m s^{-2}). The background field is the radial velocity field observed by the CP-3 radar at $z = 600$ m AGL and at 2022:24 UTC.

TABLE 2. Amplitude of the terms in the conservation equation for reflectivity (10^{-2} dBZ s^{-1}) and the correlation ρ between the tendency and the advection terms as function of the radius of influence used in the data analysis.

R_i (m)	$\left\vert\overline{\frac{\partial\eta}{\partial t}}\right\vert$	$\left\vert\overline{u\frac{\partial\eta}{\partial x}+v\frac{\partial\eta}{\partial y}}\right\vert$	$\left\vert\overline{\frac{\partial\eta}{\partial t}+u\frac{\partial\eta}{\partial x}+v\frac{\partial\eta}{\partial y}}\right\vert$	ρ
200	0.66	1.01	0.99	−0.27
400	0.56	0.62	0.60	−0.43
800	0.52	0.52	0.51	−0.46
1600	0.49	0.46	0.46	−0.46
3200	0.47	0.41	0.43	−0.46
6400	0.45	0.38	0.42	−0.45

is 1.31 m s^{-1}, which is lower than the 1.64 m s^{-1} obtained in experiment 5 with TREC. It seems that the VET method is able to retrieve the wind field at a finer resolution. We will see in the next section that the results can be further improved with the variational formulation.

b. *Experiments with the variational method*

As mentioned in section 3c, the η-conservation and r-momentum equations contain significant model errors. Since the dual-Doppler wind field is known, each term on the left-hand side of (4) and (16), as well as their residuals, can be calculated by inserting the observations into the equations. The model errors can be estimated directly from the residuals, although the observational errors in the dual-Doppler analysis also contribute to the residuals. These contributions are however marginal. Figures 15 and 16 show the spatial distribution of the residuals of the left-hand side of (4) and (16), respectively. Only the highest residuals are depicted to better assess the homogeneity of the distributions. The model error of the η-conservation equation is strongly anisotropic and the highest values are found in the precipitating cell region. This was expected since the reflectivity in this region is from falling precipitation and the residual of (4) has a strong component from the vertical advection. On the other hand, the model error of the r-momentum equation is fairly

TABLE 3. Amplitude of the terms in the momentum equation for radial velocity (10^{-3} m s^{-2}) and the correlation ρ between the tendency and the advection terms as function of the radius of influence used in the data analysis.

R_i (m)	$\left\vert\overline{\frac{\partial v_r}{\partial t}}\right\vert$	$\left\vert\overline{u\frac{\partial v_r}{\partial x}+v\frac{\partial v_r}{\partial y}}\right\vert$	$\left\vert\overline{\frac{\partial v_r}{\partial t}+u\frac{\partial v_r}{\partial x}+v\frac{\partial v_r}{\partial y}}\right\vert$	$\overline{\frac{v_\theta^2}{r}}$	ρ
200	1.12	2.21	2.21	0.06	−0.29
400	0.91	1.11	1.10	0.04	−0.51
800	0.84	0.89	0.81	0.04	−0.56
1600	0.79	0.77	0.71	0.04	−0.58
3200	0.75	0.69	0.65	0.03	−0.60
6400	0.72	0.64	0.61	0.03	−0.60

homogeneous. Tables 2 and 3 list the mean amplitude of the terms in (4) and (16) over the domain and the correlation between the local tendency and the advection terms for various radii of influence, R_i used in the analysis. First of all, the curvature term v_θ^2/r in the r-momentum equation is negligible. With the resolution defined by $R_i = 200$ m the mean residuals (column 4) are of the same magnitude as the advection terms and are twice the magnitude of the tendency terms in both equations. The correlation between the local tendency and the advection terms is also very poor. Ideally, if the constraining equations represented correctly the evolution of the observations, this correlation should be equal to -1. Even in clear-air echoes the forcing and the sources and sinks appear to be important. When the radius of influence increases, the mean residuals diminish but remain of the same order of magnitude as the first two terms. However, the correlations improve as R_i increases indicating that the equations can be helpful for retrieving the largest scales in the wind field. This is consistent with the results obtained with the TREC and TRED methods where large sectors were needed to find a stable solution.

The variational method is next applied to retrieve the horizontal wind field from the high-resolution analysis ($R_i = 200$ m) as in the previous experiments. The minimization algorithm is halted after 300 iterations although no improvement was observed in most experiments beyond 50 iterations. This high number of iterations was employed to ensure that the minimization is achieved in all cases. To assess the sensitivity of the retrieval to choice of the weights, we have conducted a very large number of experiments in which the weights were varied from 10^{-3} to 10^3 for k_η, k_m, and k_v and from 10^{-2} to 10^4 for γ, (all being nondimensional constants). Table 4 lists the experiments retained in the following discussion.

Here J_η or J_m can each be used alone as a constraint to retrieve the wind field. Figure 17 shows the retrieved wind when only the conservation of reflectivity is used as a constraint (experiment 11). Only the wind vectors corresponding to the ones obtained in experiments (1)–(5) and (10) are depicted for convenience. Actually, the retrieved wind field has the same resolution as the dual-Doppler analysis in Fig. 4. The wind field in Fig. 17 is compared with that from the dual-Doppler averaged over sectors of 2 km × 2 km as in the previous experiments. As expected, the retrieved wind field is very noisy and the correlation between the retrieved and the dual-Doppler tangential velocities is only 0.20. Similar results (not shown) are obtained when the r-momentum equation is used alone as a constraint.

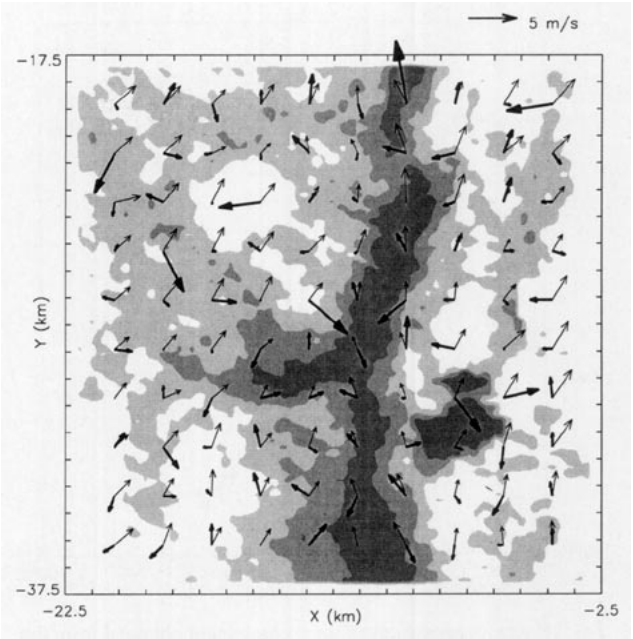

FIG. 17. Retrieved wind field (thick vectors) with the variational method when $k_\eta = 1.0$, $k_m = 0.0$, $k_v = 0.0$, and $\gamma = 0.0$. The thin vectors represent the corresponding dual-Doppler wind field averaged over arrays of 2 km × 2 km. The background field is the reflectivity observed by the CP-3 radar at $z = 600$ m AGL and $t = 2022{:}24$ UTC.

TABLE 4. Summary of experiments with the variational method. Units of the weights are nondimensional; ρ is the correlation coefficient between the retrieved and the dual-Doppler tangential velocities.

Experiment number	Weights				rmsd (v_θ) (m s^{-1})	ρ
	k_η	k_m	k_v	γ		
11	1.0	0.0	0.0	0.0	1.73	0.20
12	1.0	0.0	0.0	1000.0	1.01	0.55
13	0.0	10.0	0.0	1000.0	0.90	0.51
14	1.0	10.0	0.0	1000.0	0.89	0.60
15	1.0	10.0	10.0	1000.0	0.84	0.66
16	as experiment 15 but $k_\eta = 0.0$ in cloud				0.74	0.72

The retrievals can be further improved by removing the noise in the data. Two approaches are possible. First, a larger radius of influence can be used in the analysis to remove the small-scale anomalies in the reflectivity and radial velocity fields. Second, a smoothness constraint can be added to the cost function as suggested in section 2c. The first solution is frequently employed in the wind retrieval methods recently developed (Xu et al. 1994; Shapiro et al. 1994; Sun and Crook 1994). They demonstrated that retrievals are significantly improved when small-scale anomalies are removed during data analysis. In this case, their model better fits the large-scale features and the retrieval is not spoiled by the noise in the analysis. The main disadvantage in doing so is that the retrieval is performed in two steps: the observations are first filtered and then the model is fitted. Moreover, the filter may remove useful information even in the large-scale anomalies. The second approach is adopted here.

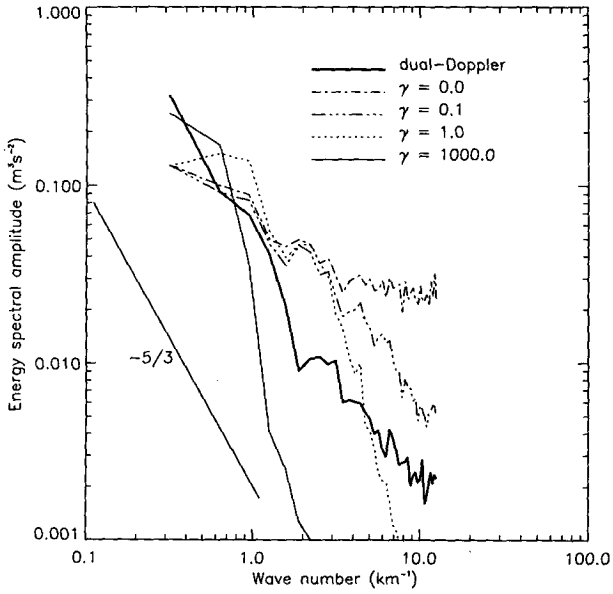

FIG. 18. Energy spectrums of the u component obtained from the dual-Doppler wind field and the retrieved wind fields for various values of γ.

Thus, the smoothness constraint, which may be considered as a low-pass filter, is a part of the model, and only one step is needed to retrieve the wind field. The scales retrieved are then controlled by the weight of the smoothness constraint.

It is interesting to observe the effect of the smoothness constraint in the frequency domain, since it indicates the scales that are properly retrieved. Figure 18 shows the power spectrum of the u component obtained from the dual-Doppler analysis (thick curve) and for different values of the weight γ. The other weights are $k_\eta = 1.0$, $k_m = 0.0$, and $k_v = 0.0$. Notice that the slope of the spectrum obtained from the dual-Doppler data follows very well the $-5/3$ law. This agrees well with the stratified turbulence theory in the mesoscale proposed by Lilly (1983). When $\gamma = 0$, the energy contained in the small-scale anomalies is very high (as expected from Fig. 17) while it is too low for the first wavenumber. Thus, the power spectrum of velocity is not well retrieved without a smoothness constraint. Compared with the dual-Doppler curve, long wavelengths are damped and short scales are enhanced. When $\gamma = 0.1$, the power spectrum at the small scale is improved while the large-scale features are almost unchanged. Increasing γ to 1.0 leads to the best, although not particularly good, overall adjustment of the power spectrum. The lowest rmsd(v_θ) is obtained when $\gamma = 1000.0$ (Table 5), the same value that optimizes the retrieval of the smallest three wavenumbers (Fig. 18). This indicates that the optimal retrieval of amplitudes *and phases* is achieved when the first three harmonics are best adjusted. The small-scale anomalies are strongly filtered while the power spectrum fits well

TABLE 5. Effect of the smoothness constraint on the rmsd(v_θ) and the correlation ρ between the retrieved and dual-Doppler tangential velocities as a function of the weight γ.

γ	rmsd(v_θ) (m s^{-1})	ρ
0.0	1.73	0.20
0.1	1.41	0.28
1.0	1.34	0.34
10.0	1.29	0.40
100.0	1.11	0.51
1000.0	1.01	0.55
10000.0	1.06	0.54

the dual-Doppler curve in the lowest wave numbers. For higher values of γ, the rate of convergence in the minimization becomes very slow and the retrievals degrade. Very similar results are obtained when the tangential velocity is considered instead of a Cartesian component.

The η-conservation equation is replaced by the r-momentum equation as a physical constraint in the experiment 13. The best retrieval is with $k_m = 10.0$, a value obtained after experimentation with several values of k_m. Also, the residuals of the r-momentum equation are one order of magnitude smaller than those of the η-conservation equation. Consequently, both constraints have the same importance when used together in the cost function. The results obtained (Fig. 20) are qualitatively comparable to the one obtained when the conservation of reflectivity is used as a physical constraint (Fig. 19). However, as shown in Table 4 the rmsd(v_θ) is about 10% lower. This is consistent

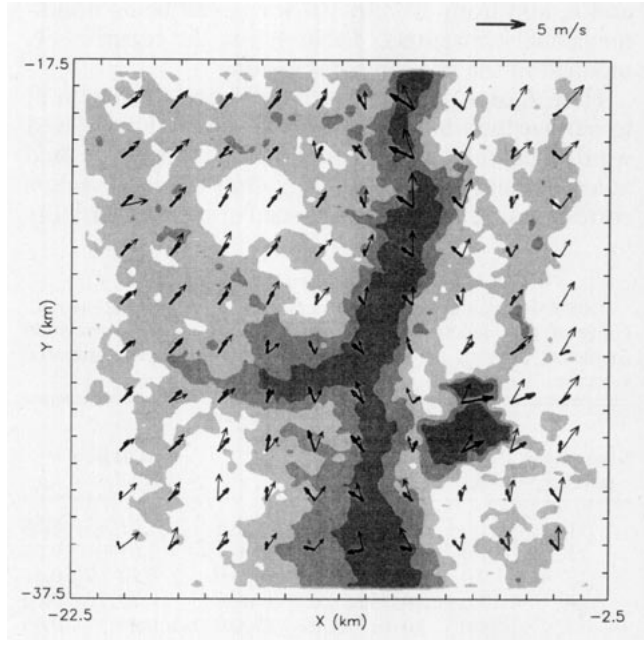

FIG. 19. Same as in Fig. 17 but when $k_\eta = 1.0$, $k_m = 0.0$, $k_v = 0.0$, and $\gamma = 1000.0$.

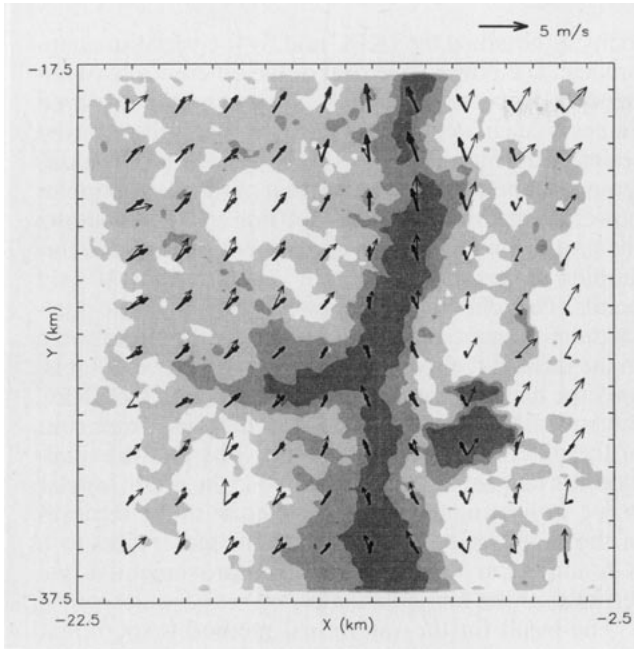

FIG. 20. Same as in Fig. 17 but when $k_\eta = 0.0$, $k_m = 10.0$, $k_v = 0.0$, and $\gamma = 1000.0$.

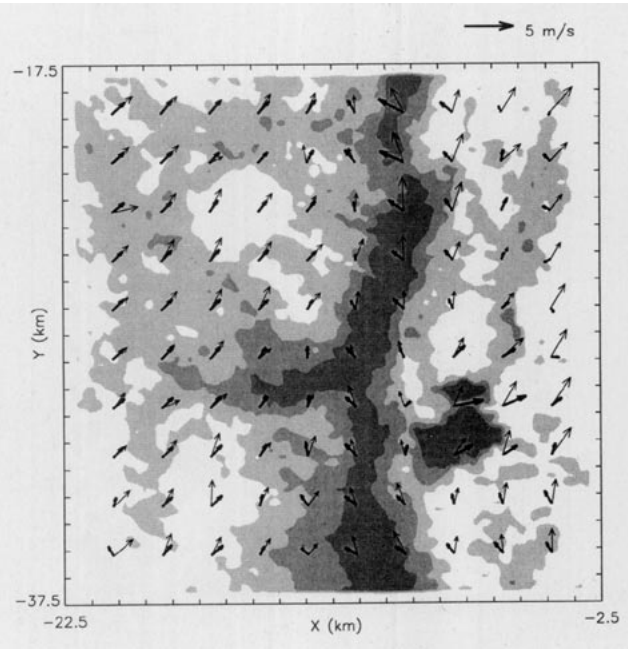

FIG. 21. Same as in Fig. 17 but when $k_\eta = 1.0$, $k_m = 10.0$, $k_v = 0.0$, and $\gamma = 1000.0$.

with the correlations between the tendency and advection terms in Tables 2 and 3 that indicate that the r-momentum equation better represents the large-scale anomalies than the η-conservation equation. In experiment 14, both physical constraints are used to retrieve the wind field (Fig. 21). Surprisingly, the results improve only slightly. It is possible that the use of constant weights hinders the potential contribution of the two independent sources of information to the quality of the retrieval. As seen in Figs. 15 and 16, the model errors are not spatially homogeneous. Therefore, the weights should be space dependent in a way that, at a given grid point, the equation with the least model error has the greatest weight and vice versa. The implementation of this procedure is not an easy task since the model errors are unknown a priori. However, according to the one-dimensional experiments in Laroche and Zawadzki (1994), errors in the retrieval are greater where the gradient of the tracer field is weaker. This property could be used to define the spatial distribution of the weights. This solution is beyond the scope of this work but should be considered in the future.

In the last two experiments, all the constraints are used to retrieve the wind field. The weight k_v is set to 10.0 as β in the VET method, which means that the difference between the retrieved and the observed radial velocity is also minimized. The other weights are set as in the previous experiment: $k_\eta = 1.0$, $k_m = 10.0$, and $\gamma = 1000.0$. As shown in Fig. 22, the wind field improves significantly since one component of the wind is constrained to be as close as possible to the corresponding dual-Doppler wind component. Nevertheless, the retrieved tangential velocity is also improved as indicated by the rmsd(v_θ) and ρ in Table 4. The largest errors in Fig. 22 are found in the rain region and in the upper right corner. The errors in the region are mainly due to the conservation of reflectivity constraint applied in two dimensions. In effect, the motion of precipitation on the horizontal plane should not be interpreted as the horizontal wind. Consequently, we

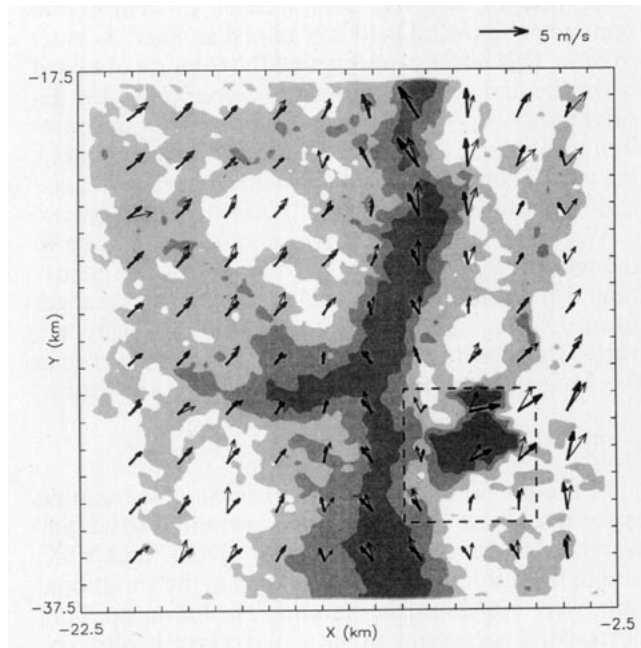

FIG. 22. Same as in Fig. 17 but when $k_\eta = 1.0$, $k_m = 10.0$, $k_v = 10.0$, and $\gamma = 1000.0$.

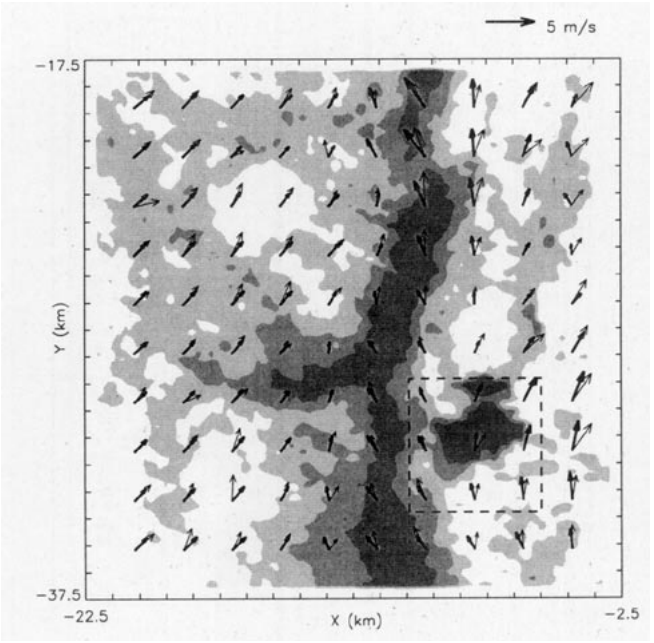

FIG. 23. Same as in Fig. 22 but $k_\eta = 0.0$ in the sector delimitated by the dashed line.

set k_η to zero in an area delimited by the dashed line in Fig. 22. As shown in Fig. 23, the retrieval is significantly improved in the precipitation region. This is also reflected in the rmsd(v_θ), which decreases to 0.74 m s^{-1} while the correlation improves to 0.72.

Another experiment is performed to test whether the absolute minimum was reached in experiment 15. For this, the first guess $\mathbf{X}_0$ is set to the dual-Doppler wind values. After the minimization procedure, the same retrieved wind field is obtained as when $\mathbf{X}_0$ is set to zero. This result confirms that the solution obtained when the first guess is set to zero converges to the desired minimum (but does not guarantee that this minimum in the cost function is unique). Unfortunately, the cost function cannot be visualized in such a large-scale minimization ($2 \times 80 \times 80$ control variables).

We found that the retrieval is quite insensitive to the weights k_η, k_m, and k_v as long as they are greater than 0.1. Indeed, for $\gamma = 1000.0$, the rmsd(v_θ) ranges from 0.84 to 1.22 m s^{-1} when the other weights are varied from 0.1 to 1000.0. When a weight is lower than 0.1, the corresponding constraint becomes ineffective.

c. *Effective resolution of the retrievals*

In the previously described retrievals, the nominal space resolution of the retrieved tangential wind corresponds to the sector size used in TREC and VET, and to the resolution of the data used in the variational approach. However, the nominal resolution does not correspond necessarily to the actual correctly retrieved scales, as we have seen in Fig. 18. Let us now compare the effective resolutions of the retrieved tangential velocity as obtained by TREC and by the variational approach. The power spectrum of the difference between the dual-Doppler tangential velocity and the retrieved values is calculated for this purpose. For well-retrieved scales (wavenumbers) the power spectrum of the differences should be well below that of the dual-Doppler power spectrum. The dash–dot line in Fig. 24 shows the results for TREC as in experiment 5 but with overlapping sectors so as to obtain values at 10×10 grid points. The solid line is the power spectrum of the dual-Doppler tangential velocity. Only the first harmonic in the dash–dot curve is below the solid curve. That is, only the first harmonic is well retrieved with the TREC method; at the shorter wavelengths the power spectrum of the difference between the retrieved and the dual-Doppler tangential velocities is above the dual-Doppler curve, indicating the presence of noise in the retrieval of the small scales. We extended the sector sizes to 6×6 and 8 km $\times$ 8 km without improvement in the retrieval of the first harmonic.

The result for the variational method (experiment 15) is shown by the long-dashed curve. The first two harmonics are now below the solid line. It appears that the first harmonic, and to a lesser extent the second harmonic, are better retrieved by the variational method. The dotted curve in Fig. 24 curve corresponds to experiment 16 (in which the constraint of conservation of reflectivity within the rain cell region is removed). The value for the second harmonic in that curve decreased appreciably, which indicates that the retrieval of the second harmonic is greatly improved. However, in spite of the low rms error in v_θ (particularly

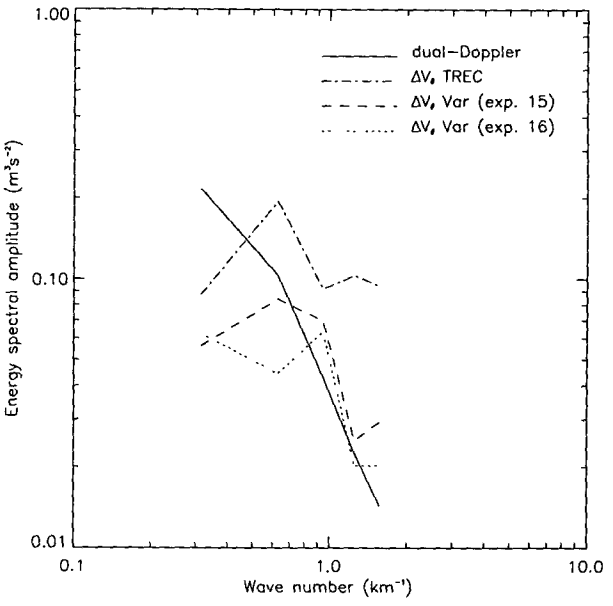

FIG. 24. Power spectrums of the difference between the dual-Doppler and the retrieved tangential velocity obtained by the TREC and the variational methods. The solid curve is the power spectrum of the dual-Doppler tangential velocity.

in experiment 16) the capability for retrieving the higher-order harmonics is nil. Thus, the variational method properly retrieves the wind structures with wavenumbers lower then 0.6 km^{-1} corresponding to wavelengths greater than 10 km. The results for TREC could be improved, at the cost of limiting the retrieval area, by removing the convective cell region.

The above analysis for the variational method well illustrates the convenience of having two constraining equations with space-dependent weights that are adjusted to the characteristics of the echo.

5. Summary and conclusions

Four methods for retrieving the horizontal wind field in the clear-air PBL from two or three time sequences of Doppler radar observations were tested using dual-Doppler data from the CaPE experiment as a test bed.

In the first series of experiments (1–7), the TREC method is compared with a similar method (TRED) that uses the conservation of reflectivity as constraint. Comparable results are obtained with both methods. The retrieval of the wind vectors from three consecutive scans is more stable than with only two scans. Of course, using three scans requires the hypothesis of stationarity to be valid over longer time periods. In the case studied here, sectors at least as large as 4 km × 4 km had to be used to obtain a stable solution. This result is consistent with the work of Tuttle and Foote (1990) who used even larger sectors of 7 km × 7 km.

In the VET method (which can be considered as an extension of TRED), the conjugate gradient algorithm is employed to minimize the difference between lagged scans. Only five iterations or less are required to find the two wind components for a given sector, which proves that the method can locate the minimum with great efficiency. However, when sectors of 4 km × 4 km are used, the cost function J_{123} sometimes contains secondary minima leading to an erroneous solution. The two constraints used in VET (conservation of reflectivity and uniform wind in the sector) are not sufficient to define a cost function having a unique minimum. The problem of multiple minima can be solved by including in the cost function an additional constraint, namely, the squared difference between the radial component of the wind and the corresponding observed radial velocity in the sector. This additional constraint also improves the retrieval of the tangential component. Finally, we find that the VET method can satisfactorily retrieve the wind field within subdomains of 2 km × 2 km.

The variational method has the advantage of incorporating several constraints to retrieve the steady-state horizontal wind field. Four constraints were used and studied: the η-conservation equation, the r-momentum equation, a smoothness constraint, and the difference between retrieved and observed radial velocity. We showed that the wind field can be satisfactorily retrieved using the η-conservation equation or the r-momentum equation only if the smoothness constraint is also added to the cost function. When the η-conservation and r-momentum equations are used together, the retrieved wind field improves only slightly. We think that the use of spatially distributed weights may further improve the retrieval. The best result is obtained when all the constraints are used with $k_\eta = 1.0$, $k_m = 10.0$, $k_v = 10.0$, and $\gamma = 1000.0$, except in the precipitation region where k_η is set to zero. In this case, the rmsd(v_θ) is 0.74 m s^{-1}, which is significantly lower than those obtained with the first three methods.

The power spectrum of the dual-Doppler data used here is consistent with well-developed homogeneous turbulence. However, we have failed to reproduce this behavior. Only two harmonics are well estimated even in the best retrieval method, the full variational approach. Whether this disappointing result is specific to this particular set of data remains to be studied. It is quite probable that in a more organized and persisting flow, one in which there is more power content in the higher-order harmonics, the retrieval of the finer scales may be possible.

Traditional methods of interpretation of single-Doppler data are based on simple and straightforward ideas and techniques. These methods have proven to be useful and robust. We have shown here that the same ideas can be combined in a unified algorithm using explicit physical constraints. The elegance and the versatility of the new approach has, however, a price: the simplicity is lost and, due to the problem of multiminima associated with the minimization of the cost function, the robustness becomes uncertain. An approach, such as the variational technique described here, can replace the traditional methods only if the problem of multiminima is solved satisfactorily. We have shown here that the addition of constraints, particularly the smoothing constraint, leads to a better conditioning of the cost function and therefore, to more reliable and consistent results.

Acknowledgments. The authors are grateful to Dr. Edward Brandes who provided us with dual-Doppler data from Florida and made some helpful comments on the manuscript. Dr. Aldo Bellon helped with a careful editing of the manuscript. The first author would like to thank the Atmospheric Environment Services of Canada for its financial support.

REFERENCES

Barnes, L. S., 1964: A technique for maximizing details in numerical weather map analysis. *J. Appl. Meteor.*, **3**, 396–409.

Brown, R. A., and V. T. Wood, 1991: On the interpretation of single-Doppler velocity patterns within severe thunderstorms. *Wea. Forecasting*, **6**, 32–48.

Doviak, R. J., and D. S. Zrnić, 1993: *Doppler Radar and Weather Observations*. Academic Press, 562 pp.

Easterbrook, C. C., 1975: Estimating horizontal wind fields for a two-dimensional curve fitting of single Doppler radar measurements.

Preprint, *16th Radar Meteorology Conf.*, Houston, TX, Amer. Meteor. Soc., 414–416.

Gray, B. M., 1991: CaPE experiment proceeds in Florida. *Bull. Amer. Meteor. Soc.*, **72,** 1287.

Laroche, S., and I. Zawadzki, 1994: A variational analysis method for the retrieval of three-dimensional wind field from single-Doppler radar data. *J. Atmos. Sci.*, **53,** 2664–2682.

Lilly, K. D., 1983: Stratified turbulence and the mesoscale variability of the atmosphere. *J. Atmos. Sci.*, **40,** 749–761.

Navon, I. M., and Legler, D. M., 1987: Conjugate-gradient method for large-scale minimization in meteorology. *Mon. Wea. Rev.*, **115,** 1479–1502.

Powell, M. J. D., 1977: Restart procedures for the conjugate gradient method. *Math. Prog.*, **12,** 241–254.

Qiu, C. J., and Q. Xu, 1992: A simple adjoint method of wind analysis for single-Doppler data. *J. Atmos. Oceanic Technol.*, **9,** 588–598.

Rinehart, R. E., 1979: Internal storm motions from a single non-Doppler weather radar. Tech. Note, NCAR/TN-146+STR, 262 pp. [Available from National Center For Atmospheric Research, P.O. Box 3000, Boulder, CO 80307-3000.]

Shapiro, A., 1993: A single-Doppler velocity retrieval in the convective planetary boundary layer. Preprint, *26th Int. Conf. on Radar Meteorology,* Norman, OK, Amer. Meteor. Soc., 441–443.

Smythe, G. R., and D. S. Zrnić, 1983: Correlation analysis of Doppler radar data and retrieval of the horizontal wind. *J. Climate Appl. Meteor.*, **22,** 297–311.

Sun, J., and A. Crook, 1994: Wind and thermodynamic retrieval from single-Doppler measurements of a gust front observed during Phoenix II. *Mon. Wea. Rev.*, **122,** 1075–1091.

——, D. W. Flicker, and D. K. Lilly, 1991: Recovery of three-dimensional wind and temperature fields from simulated single-Doppler radar data. *J. Atmos. Sci.*, **48,** 876–890.

Thacker, W. C., 1988: Fitting models to inadequate data by enforcing spatial and temporal smoothness. *J. Geophys. Res.*, **93,** 10 655–10 665.

Tuttle, J. D., and G. B. Foote, 1990: Determination of the boundary layer airflow from single Doppler radar. *J. Atmos. Oceanic Technol.*, **7,** 218–232.

Wahba, G., and J. Wendelberger, 1980: Some new mathematical methods for variational objective analysis using splines and cross validation. *Mon. Wea. Rev.*, **108,** 36–57.

Waldteufel, A., and H. Corbin, 1979: On the analysis of single-Doppler radar data. *J. Appl. Meteor.*, **18,** 532–542.

Xu, Q., C. J. Qiu, and J. X. Yu, 1994: Adjoint-method retrievals of low-altitude wind fields from single-Doppler wind data. *J. Atmos. Oceanic Technol.*, **11,** 579–585.

Zawadzki, I. I., 1973: Statistical properties of precipitation patterns. *J. Appl. Meteor.*, **12,** 459–472.